CLASSIFICATION OF TREE SPECIES AT THE LEAF LEVEL BASED ON HYPERSPECTRAL IMAGING TECHNOLOGY[**]

R. Yang, J. Kan*

School of Technology, Beijing Forestry University, Beijing 100083, China
Key Laboratory of State Forestry Administration on Forestry Equipment and Automation, Beijing 100083, China; e-mail: kanjm@bjfu.edu.cn

This study utilized hyperspectral imaging technology to identify eight tree species at the leaf level. The successive projections algorithm (SPA), information gain (IG), and Gini index (Gini) were used to select the feature bands. Furthermore, the binary particle swarm optimization (BPSO) algorithm was used to optimize the feature bands selected by SPA, IG, and Gini. The particle swarm optimization-extreme learning machine (PSO-ELM), linear Bayes normal classifier (LBNC), and k-nearest neighbor (KNN) recognition models for tree species were established based on all bands, feature bands, and optimized feature bands, respectively. The experimental results show that the recognition rates of the PSO-ELM, LBNC, and KNN models based on all bands were 98.45, 99.10, and 83.67%, respectively. The SPA, IG, and Gini can all effectively select spectral bands on tree species discrimination and greatly reduce the dimension of spectral data, in which the recognition effects of the models based on the feature bands selected by Gini were the best, and the recognition rates of the PSO-ELM, LBNC, and KNN models reached 97.55, 96.53, and 80.5%, respectively. Additionally, BPSO-SPA, BPSO-IG, and BPSO-Gini can all further reduce the dimension of spectral data on the basis of ensuring the recognition accuracy of models, in which the models established based on the optimized feature bands selected by BPSO-Gini achieved the best recognition effect and the recognition rates of the PSO-ELM, LBNC, and KNN models reached 96.53, 96.68, and 81.05%, respectively. In general, the recognition performance of the PSO-ELM model was better than those of the LBNC and KNN models.

Keywords: *tree species identification, leaf level, hyperspectral imaging technology, dimensionality reduction, feature band optimization.*

КЛАССИФИКАЦИЯ ВИДОВ ДЕРЕВЬЕВ НА УРОВНЕ ЛИСТЬЕВ НА ОСНОВЕ ТЕХНОЛОГИИ ГИПЕРСПЕКТРАЛЬНОЙ ВИЗУАЛИЗАЦИИ

R. Yang, J. Kan*

УДК 535.3:581.45

Пекинский лесотехнический университет,
Пекин 100083, Китай; e-mail: kanjm@bjfu.edu.cn

(Поступила 22 октября 2018)

Технология гиперспектральной визуализации использована для идентификации восьми пород деревьев на уровне отдельных листьев. Для выбора характерных спектральных полос использованы алгоритм последовательных проекций (SPA), коэффициент усиления информации (IG) и индекс Джини (Gini). Алгоритм оптимизации роя бинарных частиц (BPSO) применен для оптимизации набора характерных полос, выбранных с помощью SPA, IG и Gini. Машинное обучение для оптимизации роя бинарных частиц (PSO-ELM), линейные модели байесовского нормального классификатора (LBNC) и k-ближайшего соседа (KNN) для пород деревьев созданы на основе всех спектральных диапазонов, характерных полос и оптимизированных характерных полос соответственно. Показатели

[**] Full text is published in JAS V. 87, No. 1 (http://springer.com/journal/10812) and in electronic version of ZhPS V. 87, No. 1 (http://www.elibrary.ru/title_about.asp?id=7318; sales@elibrary.ru).

распознавания моделями PSO-ELM, LBNC и KNN на основе всех спектральных диапазонов составляют 98.45, 99.10 и 83.67% соответственно. Методы SPA, IG и Gini позволяют эффективно выбирать спектральные полосы для различения пород деревьев и значительно уменьшать размерность необходимых для распознавания спектральных данных. Результаты распознавания моделями, основанными на характерных полосах, выбранных Gini, лучшие, а показатели распознавания моделями PSO-ELM, LBNC и KNN достигали 97.55, 96.53 и 80.5% соответственно. BPSO-SPA, BPSO-IG и BPSO-Gini дополнительно уменьшают размерность спектральных данных, не снижая точности распознавания. Модели, созданные на основе оптимизированных характерных полос, выбранных с помощью BPSO-Gini, показывают наилучший результат распознавания, а показатели распознавания моделями PSO-ELM, LBNC и KNN составили 96.53, 96.68 и 81.05% соответственно. В целом показатели распознавания модели PSO-ELM лучше, чем моделей LBNC и KNN.

Ключевые слова: *идентификация древесных пород, уровень отдельных листьев, технология гиперспектральной визуализации, уменьшение размерности, оптимизация набора характерных полос.*

Introduction. Forest resources comprise the main body of terrestrial ecosystems and are the foundation for the construction of forest and ecological environments. In addition, they play an irreplaceable role in the sustainable development of the economy, society, and environment [1]. Knowing the tree species composition of a forest can provide valuable information for estimating the forest economic value and studying forest ecosystems [2]. It is important for forest resource management and monitoring to accurately identify tree species [3].

Hyperspectral imaging technology combines spectral technology with image technology. This technique can not only provide the image features of the spatial distribution of an object, but also obtain an abundance of spectral information for each pixel or group of pixels over the object [4]. In view of the advantages of hyperspectral imaging technology, many scholars have applied it to tree species recognition. These studies typically used satellite borne or airborne hyperspectral sensors to obtain forest canopy hyperspectral images. Feret et al. [5] identified canopy species in a Hawaiian tropical forest based on airborne imaging spectroscopy and confirmed that a combination of spectral and spatial information enabled an increase in the accuracy of species classification. George et al. [6] discriminated broadleaved evergreen and conifer forest tree species in the western Himalayas using EO-1 Hyperion data, and the results demonstrated that narrow spectral bands of Hyperion data possessed potential application value in identifying tree species. Jia et al. [7] mapped mangrove species by combining EO-1 Hyperion hyperspectral images and high-spatial-resolution SPOT-5 data using an objected-oriented method, and the overall accuracy of the mangrove map reached 88%, which indicated the great potential of using high-resolution hyperspectral data for distinguishing and mapping mangrove species. In addition, many recent studies have integrated LiDAR and hyperspectral data to identify tree species [8–10]. Hyperspectral and LiDAR data provide the possibility of combining vertical and horizontal profile information, which is a promising new method for tree species identification [11]. According to the literature, these studies were conducted to identify tree species by obtaining canopy-level hyperspectral data based on hyperspectral imaging technology. However, the challenge with passive imaging is relying on sunlight and the high impacts of variations and different illumination conditions on data radiometry [12–14]. The shadowing and brightening of individual tree crowns make the pixels of a single tree crown range from very dark pixels to very bright pixels [15], which affects the quality of hyperspectral data. In addition, there are studies that have been performed to identify tree species by obtaining leaf-level hyperspectral data based on non-imaging hyperspectral technology [16–18]. This method is also affected by natural light and weather conditions. Furthermore, non-imaging hyperspectral technology is used to obtain the hyperspectral data of a target surface by optical fiber probe. This only ensures that the target is filled with the view field of the probe, but it cannot accurately select a certain region of interest. According to the above literature and the existing problems, this study utilized hyperspectral imaging technology to obtain leaf-level hyperspectral reflectance data under an indoor halogen lamp light source to identify tree species.

Hyperspectral images contain hundreds of contiguous spectral bands and provide abundant information for classification of objects [19, 20]. However, high-dimensional hyperspectral data increase the cost of data collection, transmission, storage, and management [21], and the adjacent hyperspectral bands are highly correlated [22]. Therefore, hyperspectral dimensionality reduction is necessary for subsequent data processing. In this paper, three dimensionality reduction algorithms, i.e., the successive projections algorithm (SPA), information gain (IG), and Gini index (Gini), were used to select feature bands to reduce the dimension of hyperspectral data. Binary particle swarm optimization (BPSO) was used to optimize the feature set.

This paper proposes a new method for tree species recognition at the leaf level based on hyperspectral imaging technology and a method for secondary screening feature bands. The specific objectives of this study were (1) to test and compare the recognition performances of different recognition models established based on all bands and feature bands using hyperspectral imaging technology and (2) to utilize the binary particle swarm optimization (BPSO) algorithm to optimize the selected feature bands and analyze the recognition performance for tree species based on the optimized feature bands.

Experimental. In this study, eight kinds of tree species (*Forsythia suspensa, Hibiscus syriacus, Cerasus serrulata, Malus micromalus, Sophora japonica, Syringa oblata Lindl., Lonicera maackii*, *and Ilex chinensis Sims*) were identified based on hyperspectral imaging technology. The leaves of these eight tree species were collected on the campus of Beijing Forestry University in summer. Five trees were selected for each tree species, and leaves were randomly collected from each tree. The collected leaves were put into sealed bags, then placed in a fresh-keeping box, and brought back to the laboratory to acquire hyperspectral images. Each leaf was taken as a sample. The samples were randomly divided into a training set (260) and test set (126) according to the proportion 2:1. The division of the tree species samples is shown in Table 1.

TABLE 1. The Division of the Tree Species Samples

Tree species	Assigent	Training set	Test set
Forsythia suspensa	1	34	16
Hibiscus syriacus	2	34	16
Cerasus serrulata	3	32	16
Malus micromalus	4	32	16
Sophora japonica	5	29	14
Syringa oblata Lindl.	6	33	16
Lonicera maackii	7	32	16
Ilex chinensis Sims	8	34	16

In this study, a SOC710VP portable hyperspectral imaging spectrometer was used to obtain the hyperspectral images of leaves, with a size of 696×520 pixels. The spectral range is 370–1042 nm, with 128 bands and a spectral resolution of 4.6875 nm. The hyperspectral imaging spectrometer possesses a built-in translation push-scan camera, which eliminates the need for an additional scanning station. The scanning speed and integral time are automatically matched without manual adjustment, which eliminates image distortion. At the time of acquiring the hyperspectral images under the halogen lamp source in the laboratory, each leaf was placed directly below the lens of the spectrometer, and the front of each leaf faced up. The height of the spectrometer was adjusted to allow the entire leaf to be within the field of view of the spectrometer. Black paper was used as the background to avoid the effect on the reflection spectra.

To eliminate the influence of the uneven distribution of light source intensity at each band and the noise generated by the dark current in the camera on the spectral data, the original image obtained should be corrected before processing. The hyperspectral image correction formula is as follows:

$$I = \frac{I_0 - I_D}{I_W - I_D}, \tag{1}$$

where I and I_0 represent the corrected and original hyperspectral images of the sample, respectively; I_D represents the dark reference image, which can be automatically obtained and saved by the imaging spectrometer applied in this study; and I_W represents the white reference image obtained from a standard white correction board, with a reflectivity of 99%.

The selection of a region of interest (ROI) in hyperspectral images is very important because it significantly affects the extraction of spectral data, and image segmentation is key to the selection of the ROI [23]. In this study, threshold segmentation was used to select the entire leaf as the ROI. The leaf image at the 733.15 nm band was selected for threshold segmentation because the image at this band can be clearly separated from the background. After threshold segmentation, the reflectance spectra of all pixels on the leaf were extracted at each band, and the average value was taken as the reflectance spectra of each band.

This study utilized the successive projections algorithm (SPA), information gain (IG), and the Gini index (Gini) to select feature bands for the classification of tree species.

The SPA is a forward selection algorithm that employs a simple projection operation in each band to select the feature bands. The feature bands selected by the SPA possess the characteristics of small collinearity and low redundancy, which represent the spectral information of most samples [24]. This algorithm has been widely used in spectral data analysis [25, 26]. In this study, the number of feature bands selected by the SPA was set in the range of 10 to 30.

IG is an important index in feature selection. It is defined by how much information a feature can bring to the classification system. The more information a feature brings, more important the feature [27].

Gini is an impurity attribute splitting method proposed by Breiman in 1984. This method has been widely used in decision tree algorithms, such as the classification and regression tree (CART), supervised learning in quest (SLIQ), and scalable parallelizable induction of classification tree (SPRINT), which are suitable for class, binary, continuous numerical fields, and other types of fields [28].

Recognition models. *Extreme learning machine.* Extreme learning machine (ELM) is a single hidden layer feedforward neural network (SLFN) proposed by Huang Guangbin [29]. This algorithm consists of three neural network layers, i.e., input layer, hidden layer, and output layer. ELM randomly generates the input weight and the hidden layer bias without constant adjustment during the training process. When the activation function $g(x)$ and the number of hidden layer neurons are set, the output weight of ELM can be uniquely determined. According to [30], the mathematical model of ELM is as follows.

Suppose that a training dataset contains N distinct samples, and each sample consists of n inputs and m outputs (i.e., $X = \{(x_i, y_i) \big| x_i = (x_{i1}, \cdots x_{in}), y_i = (y_{i1}, \cdots, y_{im}), i = 1, \cdots, N\}$). The specific mathematical model is expressed as

$$\underset{N\times L}{H}\ \underset{L\times m}{\beta} = \underset{N\times m}{T}, \tag{2}$$

where H represents the hidden layer output matrix, i.e.,

$$\underset{N\times L}{H} = \begin{bmatrix} g(w_1 x_1 + b_1) & \cdots & g(w_L x_1 + b_L) \\ \vdots & \ddots & \vdots \\ g(w_1 x_N + b_1) & \cdots & g(w_L x_N + b_L) \end{bmatrix}, \tag{3}$$

where $w = [w_1, \cdots, w_L]$ represents the input weight, $b = [b_1, \cdots, b_L]$ represents the hidden layer bias, and L represents the number of hidden layer neurons. β represents the output weight matrix, i.e.,

$$\underset{L\times m}{\beta} = \begin{bmatrix} \beta_{11} & \cdots & \beta_{1m} \\ \vdots & \ddots & \vdots \\ \beta_{L1} & \cdots & \beta_{Lm} \end{bmatrix}, \tag{4}$$

T represents the target output matrix, i.e.,

$$\underset{N\times m}{T} = \begin{bmatrix} y_{11} & \cdots & y_{1m} \\ \vdots & \ddots & \vdots \\ y_{N1} & \cdots & y_{Nm} \end{bmatrix}. \tag{5}$$

In the model, T is determined by prior knowledge, so when H is determined; β can be obtained using to solve

$$\min_{\beta} \left\| H\beta - T \right\|, \tag{6}$$

$$\hat{\beta} = H^{\dagger} T, \tag{7}$$

where $H^{\dagger}$ represents the Moore-Penrose generalized inverse of H.

Linear Bayes normal classifier. The linear Bayes normal classifier (LBNC) is a linear classifier based on a normal probability density with an equal covariance matrix. The class with the maximum posterior probability is selected as the class to which the object belongs. This method assumes that all feather attributes of each class obey a multidimensional normal distribution and that the covariance matrix of each class is the same. This classifier follows the Bayes decision theory [31], and its specific principles are as follows:

$$P(\omega_i \big| x) = \frac{p(x \big| \omega_i) P(\omega_i)}{\sum_{i=1}^{c} p(x \big| \omega_i) P(\omega_i)}, \tag{8}$$

where c represents the number of classes, and $P(\omega_i|x)$ represents the a posteriori probability of the sample x assigned to the class ω_i; $P(\omega_i)$ represents the a priori probability of class ω_i

$$P(\omega_i) = n_i/n, \tag{9}$$

where n_i represents the number of training samples belonging to the class ω_i and n represents the total number of training samples; $p(x|\omega_i)$ represents the class conditional probability density function of the sample x given ω_i,

$$p(x|\omega_i) = \frac{1}{\sqrt{(2\pi)^D |\Sigma_i|}} \exp(-\frac{1}{2}(x-\mu_i)^T \Sigma_i^{-1}(x-\mu_i)), \tag{10}$$

where Σ_i represents the covariance matrix of class ω_i assuming that the covariance matrix of each class is the same (i.e., $\Sigma_1 = \Sigma_2 = \ldots \Sigma_c$); μ_i represents the mean vector of class ω_i, and D represents the dimension of the sample attributes.

K-nearest neighbor. The k-nearest neighbor (KNN) is a simple and intuitive machine learning classifier proposed by Cover and Hart [32]. The basic concept of the KNN lies in calculating the distance between the unknown class sample and all training samples in the high-dimensional space by the distance function and selecting k training samples with the smallest distance from the unknown-class sample as the k nearest neighbor. The class with the largest number of occurrences in the k nearest neighbor is taken as the class of the unknown class sample. Therefore, the neighborhood value k is a key parameter of the KNN classifier, and it has a significant impact on the classification results. In this study, the Euclidean distance is used as the distance function:

$$D(X,Y) = \sqrt{(x_1-y_1)^2 + (x_2-y_2)^2 + \cdots + (x_n-y_n)^2} = \sqrt{\sum_{i=1}^{n}(x_i-y_i)^2}. \tag{11}$$

Optimization. The input weight and hidden layer bias in the ELM model are randomly generated, which has a certain effect on the recognition performance of the ELM. According to the literature [33], the particle swarm optimization (PSO) algorithm was utilized to optimize the ELM to obtain the optimal input weight and hidden layer bias, named PSO-ELM. In addition, to further mine effective information on the spectral data, the binary particle swarm optimization (BPSO) algorithm was used to optimize the selected feature bands in this study.

Particle swarm optimization algorithm. Particle swarm optimization (PSO) is an optimization algorithm for simulating bird foraging behavior, as proposed by Kennedy and Eberhart in 1995 [34]. In the PSO, a batch of particles is initialized. Each particle contains position and velocity information. The position of the particle represents the candidate solution of the problem to be optimized, and the fitness function of the position to the optimization target is used to evaluate the quality of the particle. The velocity determines the movement direction and speed of the particle. These particles search for optimal solutions in the search space by moving and communicating with each other. The velocity and position of each particle are updated by the equations

$$v_{id}^{k+1} = wv_{id}^{k} + c_1 r_1 (pbest_{id}^{k} - x_{id}^{k}) + c_2 r_2 (gbest_{d}^{k} - x_{id}^{k}), \tag{12}$$

$$x_{id}^{k+1} = x_{id}^{k} + v_{id}^{k+1}, \tag{13}$$

where v_{id}^{k} and x_{id}^{k} are the velocity and position of particle i in dimension d at the kth iteration, respectively; c_1 and c_2 are the acceleration constants; r_1 and r_2 are random values distributed within [0,1]; $pbest_{id}^{k}$ represents the optimal position of the d^{th} dimension of particle i at the kth iteration; and $gbest_{d}^{k}$ represents the optimal position of dth dimension in the whole particle swarm. To prevent the blind search of particles, the position and velocity are usually limited within a certain range (i.e., $x_{id}^{k} \in [-x_{\max}, x_{\max}]$ and $v_{id}^{k} \in [-v_{\max}, v_{\max}]$), and w represents the inertia weight, which is automatically adjusted according to

$$w = w_{\min} + \frac{(w_{\max} - w_{\min})(Maxiter - k)}{Maxiter}, \tag{14}$$

where *Maxiter* represents the number of iterations in the PSO.

In this study, the position and velocity of each particle in each dimension are limited at [–1,1]. The specific settings of the parameters for the PSO are shown in Table 2. In addition, the error recognition rate of the ELM model in the test set was taken as the fitness value of particle. The smaller the fitness value of the particle, the better the quality of the particle.

TABLE 2. Parameter Settings for the PSO

Parameters	Value
Maxiter	200
Population size	10
c_1, c_2	1.49445
w_{max}	0.9
w_{min}	0.4

Binary particle swarm optimization algorithm. PSO was initially used to solve optimization problems in continuous space. To solve the combinatorial optimization problem, a binary particle swarm optimization (BPSO) algorithm was proposed by Kennedy and Eberhart in 1997 [35]. In BPSO, the position of each particle in each dimension is represented by only 0 or 1. In the application of feature combinations, the number 1 indicates that the feature corresponding to the position is selected, and the number 0 indicates that it is not selected. The speed of each particle in each dimension is converted to the probability value by the Sigmoid function

$$sig(v_{id}^k) = \frac{1}{1+\exp(-v_{id}^k)}, \tag{15}$$

Equation (15) indicates the probability that the dth dimension takes the value 0 or 1. The position of each particle is updated according to

$$x_{id}^k = \begin{cases} 0, & r \geq \text{sig}(v_{id}^k) \\ 1, & r < \text{sig}(v_{id}^k) \end{cases}, \tag{16}$$

where r represents a random value distributed within [0,1]. The velocity of each particle in BPSO is updated in the same way as that in the PSO algorithm, as shown in Eq. (9).

In BPSO, the settings of the parameters were the same as those of PSO, as shown in Table 2. In addition, the error recognition rates of PSO-ELM, LBNC, and KNN models in the test set were taken as the fitness values of the particles under the corresponding models.

Results and discussion. The spectral range of the spectrometer used in this study is 370–1042 nm. Since the raw hyperspectral data contained a large amount of random noises at both ends of the distribution [36], the spectra between 400–1000 nm, with 114 bands, were intercepted for subsequent analysis. All leaf spectra of each tree species were averaged in the training set to plot the raw average reflectance spectral curve for each tree species, as shown in Fig. 1a. There are many obvious dips and spikes in the near-infrared region 750–950 nm of the raw spectra, which affects the accuracy of the recognition models. Therefore, Savitzky-Golay smoothing (SG) was used to preprocess the raw spectra in all bands. The average spectral curve after pretreatment is shown in Fig. 1b. By comparing Fig. 1a and Fig. 1b, it can be seen that the dips in the spec-

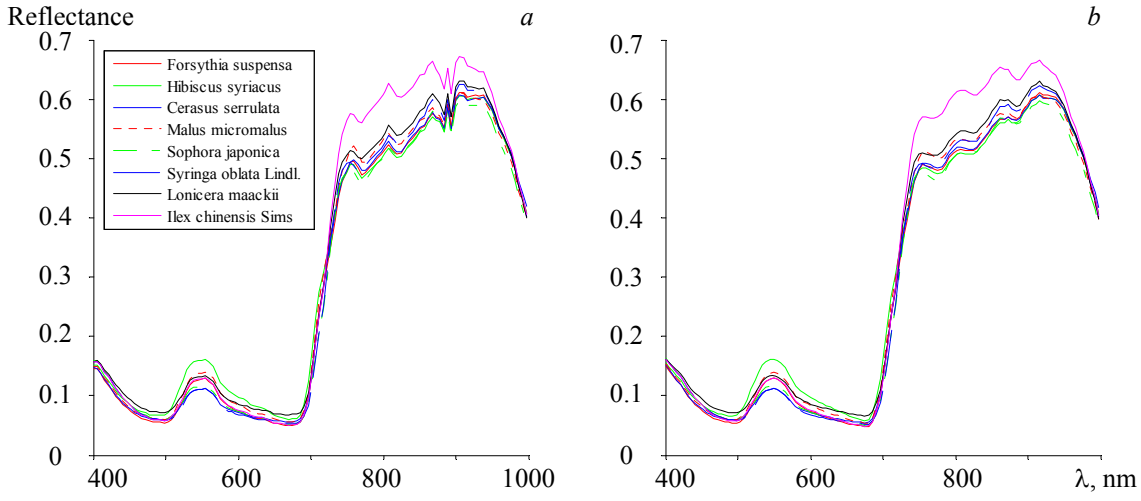

Fig. 1. The raw (a) and smooth (b) spectral reflectance of the leaves for each tree species.

tral curve are significantly reduced, and the smoothness is improved after SG pretreatment, which indicates that SG can effectively smooth high frequency noises. Therefore, the preprocessed spectral data were used for subsequent studies. In addition, the reflectance spectral curve trends for each tree species are basically the same, but the reflectivity varies from species to species. Therefore, the identification of different tree species requires further modeling and analysis.

This study utilized the SPA, IG, and Gini to select feature bands for the classification of tree species. The SPA employed a simple projection operation of each band to select the feature bands. The IG is used to select the bands corresponding to the peak values of the information gain curve as the feature bands. Gini selects the bands corresponding to the valley values of the Gini index curve as the feature bands. The results of the feature band selection are shown in Fig. 2 and Table 3. The number of feature bands selected based on the SPA, IG, and Gini was 18, 14, and 22, respectively. Compared with the 114 spectral bands, the dimension of the spectral data was greatly compressed after the selection of feature bands.

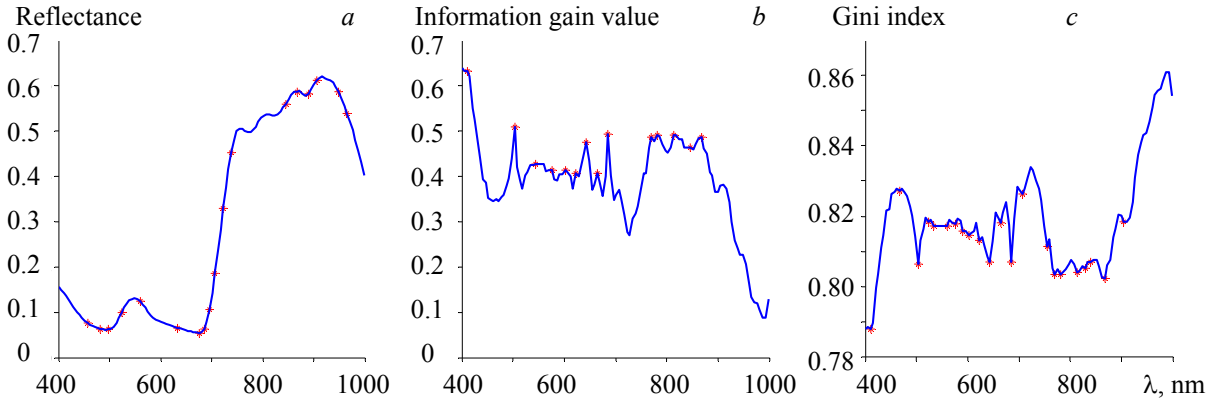

Fig. 2. The selected feature bands (*) based on SPA (a), IG (b), and Gini (c).

TABLE 3. The Results of the Feature Band Selection Based on all Bands

Method	Selected feature bands, nm	Number of feature bands
SPA	456.66, 482.29, 497.72, 523.50, 559.76, 632.82, 674.90, 685.46, 696.03, 706.62, 722.53, 738.47, 845.63, 867.24, 888.91, 905.20, 948.81, 965.23	18
IG	410.75, 502.87, 544.20, 575.35, 601.42, 622.34, 643.32, 664.36 ,685.46, 770.46, 781.15, 813.32, 845.63, 867.24	14
Gini	410.75, 466.90, 502.87, 523.50, 533.84, 559.76, 575.35, 590.98,601.42, 622.34, 643.32, 664.36, 685.46, 706.62, 754.45, 770.46, 781.15, 813.32, 829.46, 840.23, 867.24, 905.20	22

Before optimizing the input weight and hidden layer bias of ELM, the activation function and the number of hidden neurons need to be set. In this paper, the Sigmoid function was used as the activation function

$$g(x) = 1/(1 + e^{-x}). \quad (17)$$

Moreover, the influence of different numbers of hidden neurons (from 5 to 250 in intervals of 5) on ELM recognition performance was analyzed. ELM randomly generates input weights and hidden layer bias, which makes the results slightly different for each run. To reduce the influence of random errors, the average value of 50 running results in the test set was taken as the evaluation criterion for ELM recognition performance. As seen from Fig. 3, ELM achieves the optimal performance when the number of hidden neurons reaches about 60.

For the KNN algorithm, the neighborhood value k is a key parameter. In the experiment, the KNN model was established under different k values ranging from 1 to 30 in intervals of 1, and the recognition rate of the test set was taken as the evaluation criterion for KNN recognition performance to find the optimal neighborhood value k. It can be seen from Fig. 4 that the recognition performance of the KNN shows a general downward trend with increase in the k value. Therefore, in this paper, the neighborhood k value was set to 1.

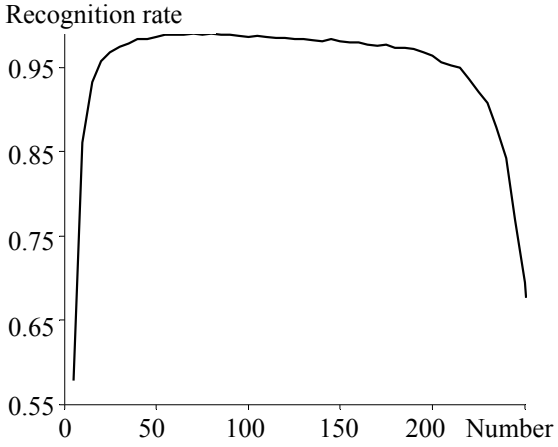

Fig. 3. The influence of the number of hidden neurons on the ELM recognition performance.

Fig. 4. The influence of the neighborhood *k* value on the KNN recognition performance.

It should be emphasized that the optimal number of hidden neurons and the neighbor *k* value were obtained based on the 400–1000 smooth spectral data. To ensure the consistency of the test conditions for the feature bands, the number of hidden neurons in the ELM models was set to 60, and the *k* values of KNN models were set to 1.

Identification results. In this study, 5-fold cross-validation was used to test the recognition effects of the PSO-ELM, LBNC, and KNN models based on all bands and feature bands. For each model, fifty runs of 5-fold cross-validation were conducted using all samples (386 samples), and the average value of the test accuracy of the fifty 5-fold cross-validation runs was used as the recognition rate for each model. In addition, the standard deviation in the test accuracy of the fifty 5-fold cross-validation runs were used to evaluate the stability of each model. The results are shown in Table 4.

TABLE 4. The Identification Results (Cross validation) Based on all Bands and Feature Bands

Method	All bands (*N*=114)		SPA (*N*=18)		IG (*N*=14)		Gini (*N*=22)	
	Recognition rate, %	Standard deviation	Recognition rate, %	Standard deviation	Recognition rate, %	Standard deviation	Recognition rate, %	Standard deviation
PSO-ELM	98.45	0.0038	97.88	0.0041	94.86	0.0083	97.55	0.0050
LBNC	99.10	0.0038	96.49	0.0056	93.94	0.0061	96.53	0.0054
KNN	83.67	0.0117	80.22	0.0092	77.52	0.0125	80.50	0.0112

N o t e: *N* is the number of feature bands.

Based on all bands, the recognition rates of the PSO-ELM, LBNC, and KNN models were 98.45, 99.10, and 83.67%, respectively. Compared with the results of all bands, the recognition results of the three models based on the feature bands extracted by SPA, IG, and Gini have slightly decreased by 0.58 to 7.35%, but the dimension of the spectral data has been greatly reduced by 80.7 to 87.71%.The standard deviations in the different models based on the feature sets were all very small, which indicates that the recognition performances of the models are stable. Therefore, the experimental results show that the SPA, IG, and Gini can effectively extract spectral information on tree species discrimination and improve the efficiency of information processing. By comparing the recognition results of the different feature extraction methods, it can be seen that the recognition effect of the models based on the feature bands extracted by Gini was the best, and the recognition rates of the PSO-ELM, LBNC, and KNN models reached 97.55, 96.53, and 80.5%, respectively. In addition, it can be seen from the results that the recognition performance of the PSO-ELM was better than that of the LBNC and KNN models.

Identification results of the feature sets optimized by the BPSO. To further obtain effective information from the spectral data, the BPSO algorithm was used to optimize the feature sets extracted by the SPA, IG, and Gini in this study. The results are shown in Table 5.

TABLE 5. The Identification Results (Cross validation) Based on Feature Sets Optimized by the BPSO

Method	BPSO-SPA			BPSO-IG			BPSO-Gini		
	Feature band number	Recognition rate, %	Standard deviation	Feature band number	Recognition rate, %	Standard deviation	Feature band number	Recognition rate, %	Standard deviation
PSO-ELM	11	96.84	0.0060	9	93.83	0.0057	14	96.53	0.0051
LBNC	15	95.78	0.0052	10	92.32	0.0050	13	96.68	0.0041
KNN	11	79.71	0.0089	8	79.69	0.0100	8	81.05	0.0118

It can be seen from Table 5 that the feature bands obtained by optimizing the same feature set using the BPSO are different in different models. The reason is that the error recognition rates of the PSO-ELM, LBNC and KNN models in the test set were taken as the fitness values of the particles in the corresponding models when using the BPSO to optimize the feature sets. After optimization, the dimension of the spectral data was further reduced, and the recognition rates of the PSO-ELM, LBNC, and KNN models based on the feature bands extracted by the BPSO-SPA, BPSO-IG, and BPSO-Gini were quite similar to those of the models based on the feature bands extracted by the SPA, IG, and Gini, respectively. In addition, the standard deviations in the different models were all very small. These results indicate that the BPSO is effective in optimizing the feature sets on the basis of ensuring model recognition accuracy. By comparing different optimized feature sets, the models based on the feature bands extracted by BPSO-Gini achieved the best recognition effect, where the recognition rates of the PSO-ELM, LBNC, and KNN models were 96.53, 96.68, and 81.05%, respectively. According to the results of the models established based on the optimized feature sets, the recognition performance of PSO-ELM was still better than those of LBNC and KNN.

Conclusion. This study utilized hyperspectral imaging technology to identify eight tree species at the leaf level and proposed a method for secondary screening of feature bands. The recognition performances of the models that were established by the PSO-ELM, LBNC, and KNN based on all bands, feature bands, and optimized feature bands, respectively, were compared. This study shows that it is feasible to identify tree species at the leaf level using hyperspectral imaging technology, and the conclusions of this study are as follows. Based on all bands, the recognition rates of the PSO-ELM, LBNC, and KNN models in the test set were 98.45, 99.10, and 83.67%, respectively. The SPA, IG, and Gini can all effectively extract the spectral information on tree species discrimination, in which the recognition effect of the models based on the feature bands extracted by Gini was the best. The BPSO-SPA, BPSO-IG, and BPSO-Gini can all further reduce the dimension of the spectral data on the basis of ensuring the model recognition accuracy, in which the models established based on the feature bands extracted by the BPSO-Gini achieved the best recognition effect. In general, the recognition performance of the PSO-ELM model was better than those of the LBNC and KNN models.

Acknowledgment. This work was supported by the National Natural Science Foundation of China (Grant No 31570713) and the Beijing Municipal Construction Project Special Fund.

REFERENCES

1. X. S. Liu, X. L. Zhang, *Forest Res. Manage*, **1**, 61–64 (2004).
2. O. Nevalainen, E. Honkavaara, S. Tuominen, N. Viljanen, T. Hakala, X. Yu, *Remote Sens*., **9**, 185 (2017).
3. L. C. Plourde, S. V. Ollinger, M. L. Smith, M. E. Martin, *Photogram. Eng. Remote Sens.*, **73**, No. 7, 829–840 (2007).
4. B. X. Ma, Y. B. Ying, X. Q. Rao, J. S. Gui, *Spectrosc. Spectr. Anal*., **29**, No. 6, 1611–1615 (2009).
5. J. B. Feret, G. P. Asner, *IEEE Transact. Geosci. Remote Sens*., **51**, No. 1, 73–84 (2012).
6. R. George, H. Padalia, S. P. S. Kushwaha, *Int. J. Appl. Earth Observ. Geoinform*., **28**, No. 1, 140–149 (2014).
7. M. Jia, Y. Zhang, Z. Wang, K. Song, C. Ren, *Int. J. Appl. Earth Observ. Geoinform*., **33**, No. 1, 226–231 (2014).
8. H. P. La, D. E. Yang, A. Chang, C. Kim, *KSCE J. Civil Engin*., **19**, No. 4, 1078–1087 (2015).
9. Z. Zhang, A. Kazakova, L. Moskal, D. Styers, *Forests*, **7**, No. 6, 122 (2016).
10. J. Cao, W. Leng, K. Liu, L. Liu, Z. He, Y. Zhu, *Remote Sens.*, **10**, No. 1, 89 (2018).
11. A. Ghosh, F. E. Fassnacht, P. K. Joshi, B. Koch, *Int. J. Appl. Earth Observ. Geoinform*., **26**, No. 2, 49–63 (2014).
12. R. D. Jackson, P. M. Teillet, P. N. Slater, G. Fedosejevs, M. F. Jasinski, J. K. Aase, *Remote Sens. Environ*., **32**, No. 2, 189–202 (1990).
13. X. Li, A. H. Strahler, *IEEE Transact. Geosci. Remote Sens*., **30**, No. 2, 276–292 (1992).
14. P. Pellikka, D. J. King, S. G. Leblanc, *Remote Sens. Rev*., **19**, No. 1-4, 259–291 (2000).
15. S. Tuominen, R. Nasi, E. Honkavaara, A. Balazs, T. Hakala, N. Viljanen, I. Polonen, H. Saari, H. Ojanen, *Remote Sens*., **10**, No. 5, 714 (2018).
16. M. A. Cochrane, *Int. J. Remote Sens*., **21**, No. 10, 2075–2087 (2000).
17. Z. H. Wang, L. X. Ding, *Spectrosc. Spectr. Analys*., **30**, No. 7, 1825–1829 (2010).
18. H. J. Lin, H. F. Zhang, Y. Q. Gao, X. Li, F. Yang, Y. F. Zhou, *Spectrosc. Spectr. Anal*., **34**, No. 12, 3358–3362 (2014).
19. X. R. Geng, K. Sun, L. Y. Ji, Y. C. Zhao, *IEEE Trans. Geosci. Remote Sens*., **52**, No. 11, 7111–7119 (2014).
20. Y. Liu, H. Xie, L. G. Wang, K. Z. Tan, *Appl. Opt*., **55**, No. 3, 462–472 (2016).
21. G. K. Zhu, Y. C. Huang, S. Y. Li, J. Tang, D. Liang, *IEEE Geosci. Remote Sens. Lett*., **14**, No. 12, 2320–2324 (2017).
22. S. Jia, G. H. Tang, J. S. Zhu, Q. Q. Li, *IEEE Trans. Geosci. Remote Sens*., **54**, No. 1, 88–102 (2016).
23. M. Huang, J. Tang, B. Yang, Q. Zhu, *Comput. Electron. Agric*., **122**, 139–145 (2016).
24. M. C. U. Araujo, T. C. B. Saldanha, R. K. H. Galvao, T. Yoneyama, H. C. Chame, V. Visani, *Chemometrics Intell. Lab. Syst*., **57**, No. 2, 65–73 (2001).
25. Q. Dai, Cheng, J. H. Sun, X. A. Zeng, *J. Food Eng*., **136**, 64–72 (2014).
26. Y. He, C. Zhang, F. Liu, W. W. Kong, P. Cui, W. J. Zhou, *Appl. Eng. Agric*., **31**, No. 1, 23–30 (2015).
27. Z. Y. Huang, *J. Shandong Agric. Univ. (Nat. Sci. Ed.)*, **44**(2), 252–256 (2013).
28. W. Q. Shang, H. K. Huang, Y. L. Liu, Y. M. Lin, Y. L. Qu, H. B. Dong, *J. Comput. Res. Dev.*, **43**(10), 1688–1694 (2006).
29. G. B. Huang, Q. Y. Zhu, C. K. Siew, *Neurocomputing*, **70**, No. 1/2/3, 489–501 (2006).
30. J. Wang, L. Zhang, J. J. Cao, D. Han, *Int. J. Mach. Learn. Cyber*., **9**, No. 1, 21–35 (2018).
31. A. Kadir, *Proc. 3rd Int. Symp*. "Leaf Identification Using Polar Fourier Transform and Linear Bayes Normal Classifier", 40–49 (**2015**).
32. T. Cover, P. Hart, *IEEE Trans. Inform. Theory*, **13**, No. 1, 21–27 (1967).
33. W. Sun, C. F. Wang, C. C. Zhang, *J. Clean Prod*., **162**, 1095–1101 (2017).
34. J. Kennedy, R. Eberhart, *IEEE Int. Conf. Neural Networks*, **4**, 1942–1948 (1995).
35. J. Kennedy, R. C. Eberhart, *IEEE Int. Conf. Systems, Man, Cybern. Comput. Cybern. Simul.*, **5**, 4104–4108 (1997).
36. X. T. Zhao, S. J. Zhang, J. L. Liu, H. X. Sun, *Food Sci. Technol*., **33**, No. 10, 281–287 (2017).